Spin wave beam driven synchronisation of nano-contact spin torque oscillators

A. Houshang[1,2], E. Iacocca[1,2], P. Dürrenfeld[1], S. R. Sani[3], J. Åkerman[1,2,3] & R. K. Dumas[1,2]

[1]*Physics Department, University of Gothenburg, 412 96, Gothenburg, Sweden*

[2]*NanOsc AB, 164 40 Kista, Sweden*

[3]*Material Physics, School of ICT, Royal Institute of Technology, Electrum 229, 164 40, Kista, Sweden*

The synchronisation of multiple nano-contact spin torque oscillators (NC-STOs) is mediated by propagating spin waves (SWs). While it has been shown that the Oersted field generated in the vicinity of the NC can dramatically alter the emission pattern of SWs, its role in the synchronisation behaviour of multiple NCs has not been considered to date. We investigate the synchronisation behaviour in multi NC-STOs oriented either vertically or horizontally, with respect to the in-plane component of the external field. Synchronisation is promoted (impeded) by the Oersted field landscape when the NCs are oriented vertically (horizontally) due to the highly anisotropic SW propagation. Not only is robust synchronisation between two oscillators observed for separations larger than 1000 nm, but synchronisation of up to five oscillators, a new record, has been observed in the vertical array geometry. Furthermore, the synchronisation can no longer be considered mutual, but driven, in nature as the final frequency is enforced by the NC-STO from which the SW beam originates.

The synchronisation of coupled non-linear oscillators is a common natural phenomenon[1].

The coupling is typically described as mutual since each oscillator plays an active role in the resulting synchronised state. Spin torque oscillators[2–7] (STOs) represent an emerging class of highly non-linear, nanoscopic, and ultra-broadband[4,8] microwave oscillators, where spin transfer torque[9–11] excites one or more spin wave modes. Mutual synchronisation is considered the primary vehicle to achieve sufficient signal quality required for applications. However, since the early seminal experiments[12,13] demonstrating spin wave (SW) based mutual synchronisation of two nanocontact STOs (NC-STOs)[14,15], progress has been relatively slow in terms of synchronising more oscillators. In 2009 four sub-GHz vortex based oscillators were synchronised through direct exchange[16], and it was not until 2013 that SW based mutual synchronisation of three high frequency NC-STOs was demonstrated[17]. In this work we investigate the impact of the NC array geometry and find that we can dramatically enhance synchronisation of up to five NC-STOs, a new record, if they are aligned perpendicular to the in-plane component of the applied magnetic field. Synchronisation is provided by a highly collimated and directional SW beam[18] arising from the Oersted field induced asymmetric field landscape[19]. As a consequence of this directionality, synchronisation can no longer be considered mutual, but driven, as the final SW mode is enforced by the NC-STO from which the SW beam originates. The demonstrated driven synchronisation has the potential to greatly increase the number of synchronised NC-STOs as one can daisy-chain an arbitrary number of NC-STOs and extend synchronisation over distances much greater than the SW propagation length.

While both localised [20–24] and propagating [23,25,26] spin wave (SW) modes can be generated in NC-STOs, it is the propagating SWs that have been shown to provide the dominant coupling

mechanism necessary to promote phase locking between NCs [27,28]. Furthermore, the role of the current induced Oersted field in the vicinity of the NC has been shown to play a critical role in SW propagation. The Oersted field not only acts to localise SW modes but, and most importantly for synchronisation, promotes a highly asymmetric propagation of SWs by locally modifying the ferromagnetic resonance (FMR) frequency[29]. When the local FMR frequency is larger than the SW frequency, propagation is thwarted, creating a so-called Oersted corral[18] effect which can result in highly collimated and directional SW beams.

To demonstrate the importance of SW beams on the synchronisation behaviour of NC-STOs we consider two NC array geometries, as shown in Fig. 1a. The NC array geometry, either vertical or horizontal, is defined with respect to the in-plane component of the external field, $H_{||}$, which points along the x-axis. The NCs have a nominal diameter of 100 nm, centre-to-centre spacing of 300 nm, and are defined on top of an all-metallic pseudo spin valve (PSV) mesa. Both scanning electron microscopy images of the NCs, and optical microscopy images of a final device showing the co-planar waveguide top contact, are shown in Fig. 1b, top and bottom, respectively. By electrical characterisation and micromagnetic simulations, we find that not only is synchronisation strongly preferred when the NCs are arranged vertically, but that the synchronisation mechanism can no longer be considered mutual. This driven, or forced, synchronisation is a direct consequence of the Oersted field induced asymmetric SW propagation. Finally, the unique magnetic field landscape generated by the vertical array also can localise, or trap, SWs in a region just outside one of the NCs.

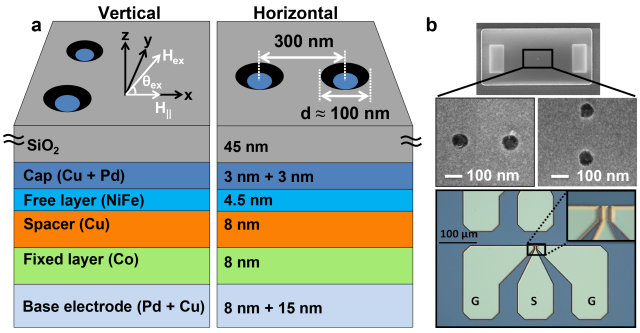

Figure 1: **Device structure.** **(a)** PSV with an all-metallic stack: Pd(8 nm)/Cu(15 nm)/Co(8 nm)/Cu(8 nm)/NiFe(4.5 nm)/Cu(3 nm)/Pd(3 nm). NC arrays are shown with vertical and horizontal arrangements with respect to the in-plane component of the external field, $H_{||}$. **(b)** Scanning electron microscopy images of the NCs with horizontal and vertical geometries, together with an optical microscopy image of the final device and the top contact coplanar waveguide, which provides electrical access to the NCs in parallel.

Results

Figure 2a shows the experimental frequency spectra of the horizontal array, measured as a function of external field angle, θ_{ex}, which is defined relative to the film plane, and a given direct current, I_{dc}. At angles larger than a critical angle, $\theta_c = 60°$, a single propagating[26] SW mode exists for each of the NCs in the free layer [23]. For angles smaller than θ_c a localised SW bullet can also be observed [22,23], in addition to other localised modes[19]. Our interest will be primarily focused on propagating SWs, and therefore $\theta_{ex} > 60°$. As can be seen in Fig. 2a, for $\theta_{ex} > 60°$ and $I_{dc} = -48$ mA, two modes with different frequencies can be observed, labelled mode 1 and 2, indicating that the NCs are not synchronised for the horizontal array at this current. The integrated power, P, and linewidth, Δf, corresponding to each of the modes are shown in Fig. 2b, for $\theta_{ex} >$

60°, with solid red and blue circles. Consistent with experiment, the inset of Fig. 2a reveals that the micromagnetically simulated phase difference, $\Delta\phi$, between the NCs (which have diameters of 100 and 90 nm to mimic the experimental variation) monotonically decreases as a function of time, indicating that synchronisation is not achieved for $\theta_{ex} = 70^\circ$. The maximum Oersted field, H_{Oe}, is roughly 10% of the external magnetic field, H_{ex}, and acts to drastically change the total field in the vicinity of the NCs. Given we consider electrons flowing into the page, the largest local field is on the bottom the NCs where H_{Oe} and $H_{||}$ point in the same direction, whereas there is a local minimum towards the upper part of the NC where $H_{||}$ and H_{Oe} oppose each other, as shown in Fig. 2d. Changes in local magnetic field then allow us to define a local variation of the FMR frequency[19] through the well-known Kittel equation. The FMR frequency, ω_0, is defined as

$$\omega_0 = \sqrt{\omega_H \left(\omega_H + \omega_M \cos^2 \theta_{int}\right)} \tag{1}$$

where $\omega_H = \gamma H_{int}$, $\omega_M = 4\pi\gamma M_S$, $\gamma = 2.8$ MHz/Oe is the gyromagnetic ratio, and M_S is the saturation magnetisation of the thin film. H_{int} and θ_{int} are the internal magnetic field and out-of-plane angle, respectively, and can be obtained by solving the magnetostatic boundary conditions for $\theta_{ex} = 70^\circ$.

The resulting variation in the FMR frequency landscape, as shown in Fig. 2c, dramatically modifies the SW propagation symmetry. A propagating SW with a frequency higher than the local FMR frequency can easily propagate into the far field [18], *i.e.* into the regions above the NCs along the $+y$ direction. Therefore, the local field landscape created by H_{Oe} promotes preferential propagation paths for the SWs, resulting in highly collimated SW beams[18]. By separately evaluating the fast Fourier transforms of each simulation cell, then then filtering each image around a

given mode frequency, the spatial profile of each mode can be mapped. This is clearly observed in Fig. 2d from the simulated SW propagation pattern for the horizontal array of NCs at $\theta_{ex} = 70^{\circ}$ and $I_{dc} = -44$ mA. Two distinct modes, which can now be assigned to each NC, with frequencies of f_{NC1}=19.5 GHz and f_{NC2}=21.1 GHz are observed. The maps are a linear scale and the intensity of the colour is proportional to the mode power. Clearly, a majority of the SW energy propagates in a direction orthogonal to the neighbouring NC which in turn significantly hampers the SW mediated mutual synchronisation mechanism described earlier. Considering all else equal, the oscillators do phase-lock for the horizontal geometry in the simulations when the NC diameters are identical [30].

A completely different behaviour is observed experimentally when the NCs are arranged vertically. Once again, for $\theta_{ex} > 60^{\circ}$, there are two modes present in the spectra, as can be seen in Fig. 3a, labelled 1+2 and X. However, the difference in frequency of the two modes is much larger ($\sim$3 GHz) and the behaviour of the integrated power and linewidth, Fig. 3b, are significantly different than the horizontal geometry, Fig. 2b. For the mode labelled 1+2 we note that the integrated power (linewidth) is much larger (smaller) than either mode observed in the horizontal geometry, consistent with a synchronised, or phase-locked, state over an angular locking range of $65^{\circ} < \theta_{ex} < 76^{\circ}$. For $\theta_{ex} < 65^{\circ}$, localisation [19] of the SW modes results in unlocking and for $\theta_{ex} > 76^{\circ}$ the role of the Oersted field in breaking the symmetry of the SW propagation is diminished, again resulting in a loss of synchronisation. Additional differences arise between the two modes when measuring the spectra as a function of current at a fixed θ_{ex}=70°, as shown in Fig. 3c. Clearly, the 1+2 mode shows a strong blue shift, i.e. as the magnitude of the current increases, so does the frequency of the oscillation mode. This is consistent with prior experiments on propagat-

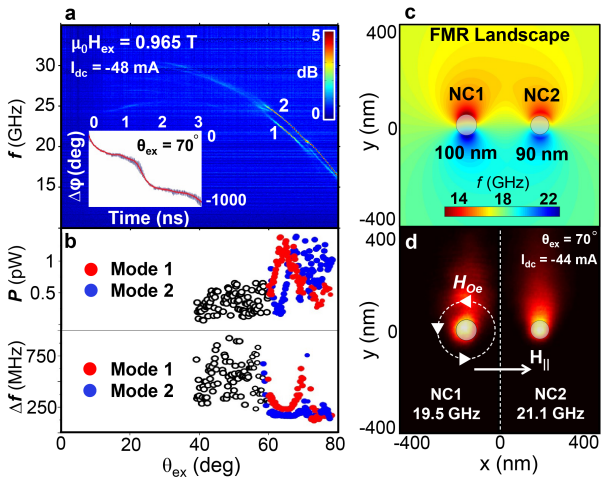

Figure 2: **Horizontal NC array characterisation.** **(a)** Experimental frequency spectra of a horizontal NC array, for $\mu_\circ H_{ex} = 0.965$ T and $I_{dc} = -48$ mA, measured as a function of external field angle, θ_{ex}. Mode 1 and 2 correspond to each of the NCs individual responses. The inset shows the simulated precessional phase difference, $\Delta\varphi$, between the NCs, indicating no synchronisation. **(b)** Experimental integrated power and linewidth of mode 1 and mode 2, solid red and blue circles, also as a function of θ_{ex}. The open symbols refer to the localised modes observed for $\theta_{ex} < \theta_c$. **(c)** The FMR frequency landscape calculated by taking into account the H_{ex} and H_{Oe} assuming electron flow into the page. **(d)** Simulated SW propagation pattern from each of the NCs for $I_{dc} = -44$ mA, $\mu_\circ H_{ex} = 0.965$ T and $\theta_{ex} = 70°$, showing highly collimated SW beams.

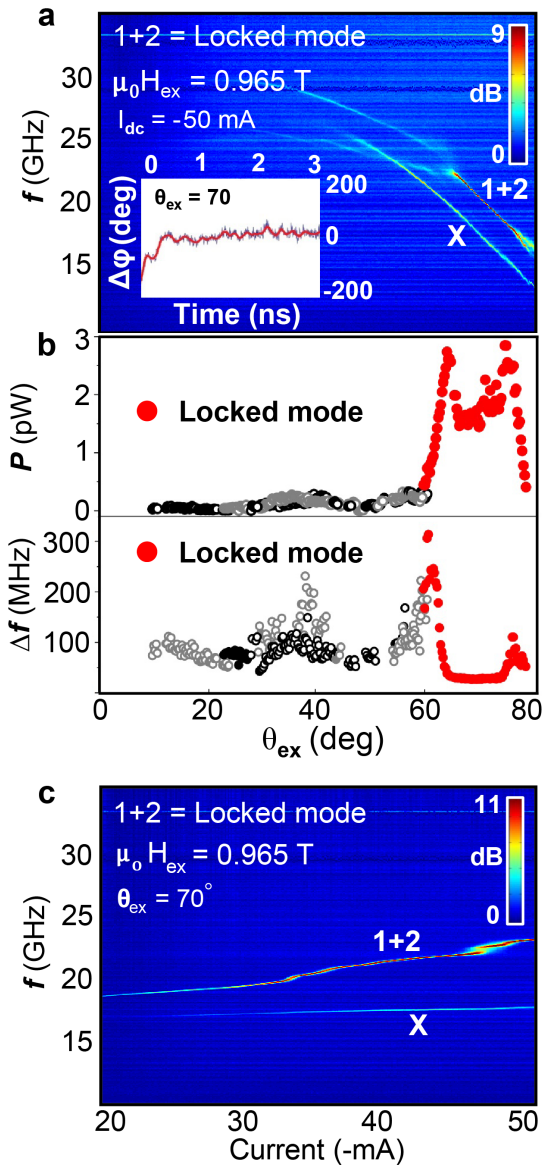

Figure 3: **Vertical NC array (a)** Experimental frequency spectra of a vertical NC array, for $\mu_\circ H_{ex} = 0.965$ T and $I_{dc} = -50$ mA, measured as a function of external field angle, θ_{ex}. Two modes, labelled 1+2 and X are found over a wide range of θ_{ex}. Mode 1+2 corresponds to the synchronised state. The inset shows the simulated precessional phase difference, $\Delta\varphi$, between the NCs, which approaches zero after a transient time period of approximately 0.5 ns, indicating a phase-locked state is achieved. **(b)** Experimental integrated power and linewidth of the 1+2 locked mode, solid red circles, measured as a function of θ_{ex}. The open symbols refer to the localised modes observed for $\theta_{ex} < \theta_c$. **(c)** Experimental frequency spectra for $\theta_{ex} = 70°$ as a function of

ing SWs for $\theta_{ex} > \theta_c$ [13,23,31]. A single 1+2 mode is also observed over the entire measurement current range, indicating a robust synchronisation in the vertical geometry. By comparison, the X mode frequency is virtually independent of bias current, suggesting a different origin. Furthermore, simulations show that $\Delta\phi$ between the NCs, seen in the inset of Fig. 3a, converges to a steady value, near 13°, consistent with a phase-locked state. In fact, the simulations also provide insights into the lower frequency X mode, and will be discussed in detail further on.

The vertical geometry produces a very different magnetic field, and therefore FMR frequency landscape, see Fig.4a, as compared to the horizontal geometry in Fig.2c. As shown in Fig. 2d, H_{Oe} promotes SW propagation upwards, and therefore the SW mediated communication between the NCs is preferred in a vertical arrangement. This is more clearly shown in Fig. 4b (blue line), which plots a single linescan from the FMR frequency landscape along $x = 0$ nm. Clearly f_{locked} (green bold line) lies above the local FMR frequency in the region between the NCs (grey regions), and therefore efficient SW mediated synchronisation is promoted. A spatial map of the simulated locked-mode frequency is shown in Fig. 4c, showing a large power under both of the NCs and a standing wave pattern[30] in the region between. A similar exercise for the X-mode, Fig. 4d, reveals that it is localised in a region just outside the lower NC and is unable to propagate due to the local FMR frequency landscape, Fig. 4b (black bold line), and is therefore also referred to as the "trapped mode".

Further details regarding the synchronisation mechanism can be elucidated by the following stepwise simulations, as outlined in Fig. 4e. Current is run through both of the NCs to ensure

the magnetic field, and therefore FMR, landscape shown in Fig. 4a is preserved. However, the spin polarisation, p, of each NC is separately controlled to find the natural frequency of each NC. Firstly, NC1 is turned on, *i.e.* p_{NC1} = 0.3 and NC2 is considered inert, *i.e.* p_{NC2} = 0. The natural frequency of NC1 is found to be $f_{NC1} = 20.48$ GHz, very close to f_{locked}, as can be seen in Fig. 4e (red). A similar exercise with only NC2 energised (p_{NC1} = 0 and p_{NC2} = 0.3) finds that NC2 has a higher natural frequency of $f_{NC2} = 21.10$ GHz, as shown in Fig. 4e (blue). Finally, when energising both NCs, (p_{NC1} = 0.3 and p_{NC2} = 0.3) we regain the synchronised state with $f_{locked} = 20.51$ GHz, as expected, Fig. 4e (green). This simple analysis has shed light on a fundamentally different synchronisation mechanism where the lower NC has the dominant role in the synchronisation process and the upper NC follows its lead. This is in stark contrast to the mutual synchronisation mechanisms previously described in which each of the NCs are equally involved in the synchronisation process[27]. In order to ensure the robustness of this mechanism, the simulations shown in Fig. 4 are repeated with the larger NC on the top, Fig. 5. Similarly, we find that synchronisation occurs at nearly the frequency of the lower NC, as can be seen in Fig. 5c and 5e.

As mentioned earlier, in addition to the locked or 1+2 mode in Fig. 3a, a second mode, labelled X, is observed. This mode can also be observed in the simulations, but only when the NCs are oriented vertically, Fig. 4d and Fig. 5d. In analogy to scanning probe FMR measurements [32], where a magnetic tip is used to generate a local field minimum in a nearby magnetic film, our H_{Oe} landscape creates a similar field profile within our free layer, as can be seen just outside of NC1 in Fig. 4b and 5b. We are able to experimentally probe the X mode as we are sensitive to

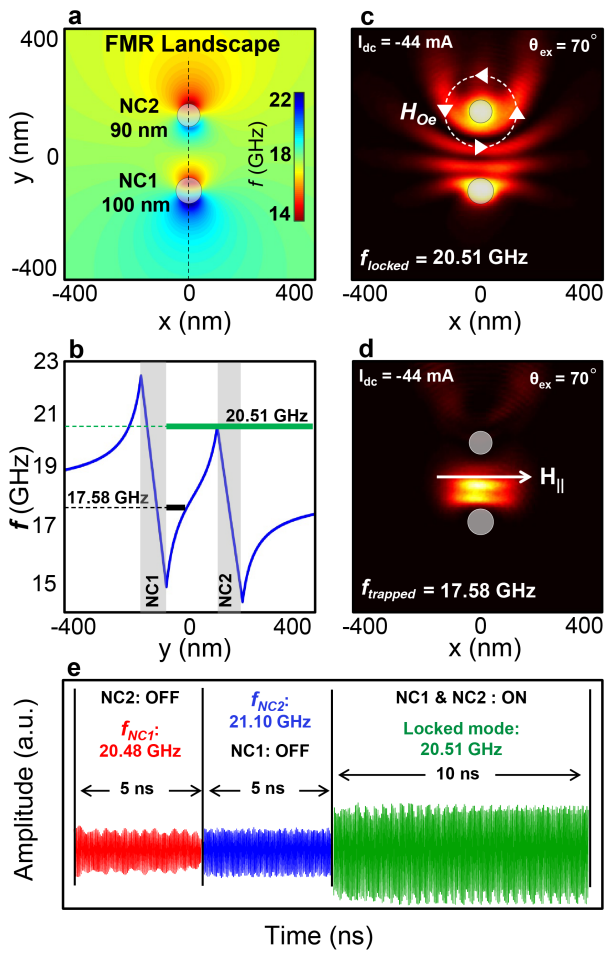

Figure 4: **Vertical NC array-simulations: Case I.** For case I the bigger, 100nm, diameter NC is located at the bottom of the NC array. **(a)** Full two-dimensional FMR frequency landscape. **(b)** One-dimensional linescan of the FMR frequency along $x = 0$. The bold green line indicates that the locked mode frequency, $f_{locked} = 20.51$ GHz, is larger than the FMR frequency in the region between the NCs whereas the bold black line indicates that the frequency of the X mode, $f_X = 17.58$ GHz, results in a localisation to a region just outside of NC1. **(c)** Spatial distribution of the phase-locked mode. **(d)** Spatial distribution of the trapped mode. **(e)** Stepwise simulations where only NC1 (red), only NC2 (blue), and both NC1 and NC2 (green) are energised. Clearly the frequency of NC1, which is towards the bottom, dominates and determines the resulting synchronised frequency.

the magnetodynamics in a region larger than the NC due to current spreading, as further quantified in supplement S1. By approximating the local field minimum with a wedge-like profile, as shown with a violet dotted line in Fig. 5b, we can calculate the expected localised SW frequencies assuming exchange dominated SWs: $f_n = (\gamma \frac{2A}{M_S}(\frac{n\pi}{m})^2)^{\frac{1}{3}} + 15.25$ GHz where A is the exchange stiffness, m is the slope (40 nm/GHz) of the wedge-shaped potential well, n is an integer, and 15.25 GHz is the bottom of the potential well. We find $f_1 \simeq 17$ GHz, in good agreement with experiment and simulations.

In Fig. 6a experimental measurements on 2-NC devices with varying centre-to-centre separations probe how far apart the separation distance between two vertically oriented NCs can be and still synchronise. Robust synchronisation is observed for centre-to-centre separations of up to 1000 nm, where only a single mode is observed. For the NCs separated by 1300 nm we have found occurrences of both synchronised and un-syncrhonised states, as we are now approaching the limit of the maximum allowed separation governed by the finite SW propagation length. Finally, all devices measured with centre-to-centre separations of 1400 nm showed two clear peaks consistent with an un-synchronised state. The loss of synchronisation for separations greater than 1300 nm is fully consistent with the experimental SW propagation length in permalloy[29] and the simulations shown in supplement S2 and S3.

Finally, experiments on devices with more than two NCs, as shown in Fig. 6b-d, have been carried out. For a NC centre-to-centre spacing of 300 nm we find robust synchronisation in 3-NC, 4-NC (Fig. 6b), and 5-NC (Fig. 6c, upper panel) devices. The average integrated power, P_{Ave}, and

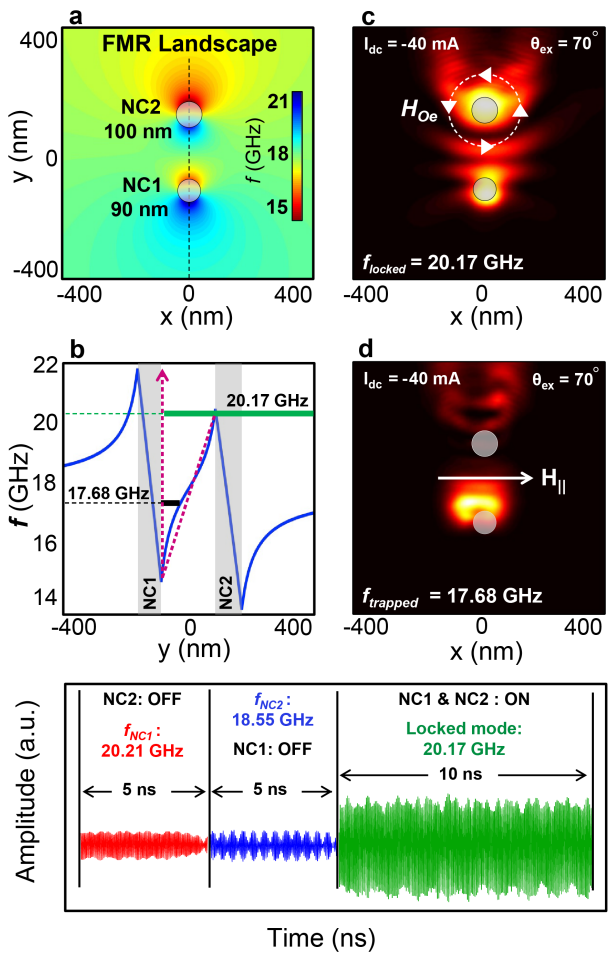

Figure 5: **Vertical NC array-Simulations: Case II.** For case II the smaller, 90 nm, diameter NC is located at the bottom of the NC array. **(a)** Full two-dimensional FMR frequency landscape. **(b)** One-dimensional linescan of the FMR frequency along $x = 0$. The bold green line indicates that the locked mode frequency, $f_{locked} = 20.17$ GHz, is larger than the FMR frequency in the region between the NCs whereas the bold black line indicates that the frequency of the X mode, $f_X = 17.68$ GHz, results in a localisation to a region just outside of NC1. The dashed violet lines indicate the shape of the potential well used in the calculation of the trapped mode frequency discussed in the text. **(c)** Spatial distribution of the locked mode. **(d)** Spatial distribution of the trapped mode. **(e)** Stepwise simulations where only NC1 (red), only NC2 (blue), and both NC1 and NC2 (green) are energised. Clearly the frequency of NC1, which is towards the bottom, dominates and determines the resulting synchronised frequency.

linewidth, Δf_{Ave}, of the 3-NC, 4-NC, and 5-NC devices are [$P_{Ave,3-NC}$=3.3 pW, $\Delta f_{Ave,3-NC}$=27.1 MHz], [$P_{Ave,4-NC}$=5.3 pW, $\Delta f_{Ave,4-NC}$=14.0 MHz] and [$P_{Ave,5-NC}$=8.5 pW, $\Delta f_{Ave,5-NC}$=11.2 MHz], respectively. Note the steady increase (decrease) of P_{Ave} (Δf_{Ave}) as the number of NCs is increased. In an attempt to break the synchronisation of the 5-NC device we have measured the spectra with an additional in-plane field angle, $\Psi_{IP} = 30^{\circ}$, shown in Fig. 6c, lower panel, where we clearly observe three distinct modes. Aided by the analysis of the integrated power and linewidth, Fig. 6d, of each mode we conclude that we have pairwise synchronisation of four of the NCs, and a single un-locked NC.

Discussion

There appears to be no fundamental limit to how many NCs can by synchronised using a vertical arrangement of NCs. To date the probability of synchronisation has followed a statistical distribution, where it has been shown for nanocontact centre-to-centre separations of 300 nm the probability of synchronisation is approximately 10%[13]. However, every device (tens of devices) measured in the vertical geometry showed robust synchronisation for separations of 300 nm. We therefore believe that by strategically taking advantage of the Oersted field induced SW beams, one can dramatically increase the output power and therefore breathe new life into the potential use of these nanoscale magnetic oscillators for a variety of oscillator applications. Another potential route would be to fabricate NCs on a predefined waveguide structure to promote and enhance synchronisation for relatively small in-plane applied fields[33]. However, utilising the driven synchronisation offered naturally by Oersted field induced SW beams is a more attractive route in terms of fabrication as

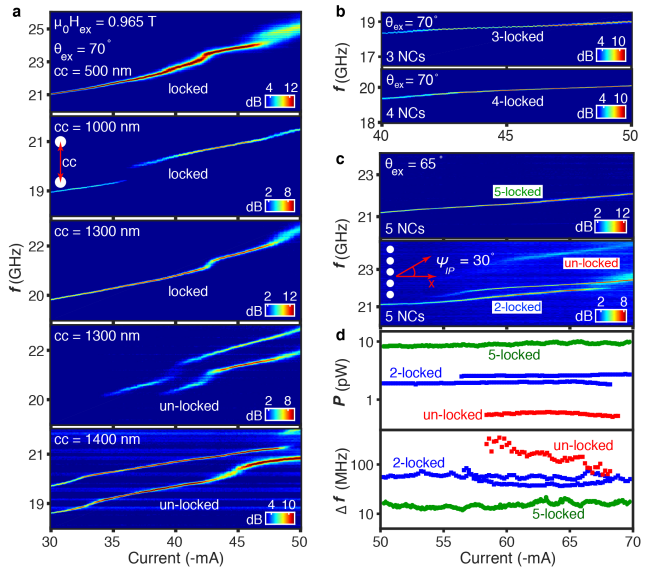

Figure 6: **Vertical NC array-Experiments: Synchronisation of two NCs with large centre-to-centre (cc) separation and synchronisation of up to 5 NCs.** **(a)** 100 nm diameter NCs with a separation of up to 1000 nm show synchronisation in all samples measured. However, for a separation of 1300 nm, both locked and un-locked states can be found depending on the particular sample. For separations larger than 1300 nm, synchronisation is never found. **(b-d)** The vertical geometry allows for robust synchronisation of more than two NCs. **(b)** 3-NC and 4-NC devices show synchronisation over the entire current range. **(c, upper panel)** Similarly, a current scan of a 5-NC device shows a single mode over the entire measured current range, indicating a locked state. **(c, lower panel)** Synchronisation can be broken by tilting the in-plane component of the applied field by 30°. **(d)** By comparing the integrated power and linewidth of the fully and partially synchronised states shown in **(c)**, we conclude that we have pairwise synchronisation of four of the NCs and a single un-locked NC in **(c, lower panel)**.

it requires no special patterning to define a waveguide. Additionally, if one aims to synchronise a very large number of NCs, connecting each oscillator in parallel with a single top contact, as opposed to relying on individual electrical control of each oscillator, is also prefereed as having separate electrical connections for more than two NCs not only becomes cumbersome in terms of fabrication but also prohibitively expensive.

In terms of potential magnonics[34] applications, one could design SW based repeaters used to transmit SW information over much larger distances than the typical SW propagation length would otherwise allow by simply daisy-chaining NCs together. Other applications include non-Boolean computation with oscillatory neural networks which operate by using the frequency-domain representation of an analogue signal where the frequency, phase, and amplitude play the role of the information carriers[35,36]. Wave based computation more easily lends itself to massively parallel computing algorithms that can even mimic neurons in the brain[37]. Similarly to STOs, neurons can be modelled as nonlinear oscillators that adjust their rhythms in response to external stimuli. In the brain they form a network of coupled oscillators where the coupling is mediated by synapses. In analogy to STOs, such neural arrays can self-synchronise. Recent progress in neuroscience has shown that neural synchronisation plays a key role in associative memory processes[38].

In conclusion, the unique magnetic field landscape generated by the vertical array creates a local field minimum that acts to localise SWs in a region just outside the NC. Furthermore, by purposefully taking advantage of the asymmetric SW propagation in NC-STOs we have not only demonstrated a new driven synchronisation mechanism, but also highlighted a simple array

geometry that can greatly increase the number of oscillators that can be synchronised. In this work synchronisation of up to 5 NCs, a new record for STOs, is demonstrated.

Methods

Experiments. The PSV used in this study is based on an all-metallic stack with the following structure: Pd(8 nm)/Cu(15 nm)/Co(8 nm)/Cu(8 nm)/$Ni_{80}Fe_{20}$(4.5 nm)/Cu(3 nm)/Pd(3 nm). The $Ni_{80}Fe_{20}$ is deposited from a stoichiometric target and simply referred to as NiFe. All the layers were deposited at room temperature using magnetron sputtering in an Ar working gas pressure of 3 mTorr on a Si/SiO_2 substrate. The base pressure of the sputtering system was lower than 5×10^{-8} Torr. After the deposition of the PSV stack, $16\ \mu m \times 8\ \mu m$ mesas were defined by conventional optical lithography. Subsequent electron beam lithography was then used to define multiple NCs with different geometries into a 45 nm thick SiO_2 layer. Electrical measurements are performed using a probe station taking advantage of a Halbach array of permanent magnets which is capable of producing a uniform and precisely rotatable field with a fixed magnitude $\mu_\circ H_{ex} = 0.965$ T. The applied field angle, θ_{ex} was swept between 0 to 80°. DC current I_{dc} is applied to the array of NCs through a bias tee and the resulting magnetodynamic response is first amplified using a low noise amplifier and measured electrically in the frequency domain using a 40 GHz spectrum analyser.

Simulations. Micromagnetic simulations were performed using the MuMax3 GPU accelerated code [39]. A disc with a diameter of 2000 nm was implemented to simulate the extended NiFe free layer. To mimic the typical experimental distribution of NC sizes, the simulated NC diameters are chosen to differ by 10%, that is diameters of 100 and 90 nm are used. Also, as our

experimental NCs are connected in parallel, we ensure each simulated NC has the same current density. A cell size of $3.9 \times 3.9 \times 5$ nm^3 together with absorbing ($\alpha = 1$) boundaries are adopted to minimise SW reflections. Simulations are performed at 300 K following Brown's thermal field formulation and the effect of the current-induced Oersted field is also included assuming the current flows along an infinite cylinder. Internal parameters used in the simulations for NiFe are a saturation magnetisation $\mu_0 M_S = 0.88$ T, exchange constant $A = 10$ pJ/m, Gilbert damping $\alpha = 0.01$ and zero magnetocrystalline anisotropy. The spin polarisation angle, which is determined from the internal magnetisation angle of the Co fixed layer, is calculated by solving the magneto-static boundary conditions and a saturation magnetisation of $\mu_0 M_{S,Co} = 1.7$ T. A spin torque efficiency of $p = 0.3$ yields a remarkable quantitative agreement with experiments. Finally, no exchange coupling between the fixed and free layer is included in our simulations.

1. Pikovsky, A., Rosenblum, M. & Kurths, J. *Synchronization: A Universal Concept in Nonlinear Sciences* (Cambridge University Press, 2003).

2. Tsoi, M. *et al.* Excitation of a magnetic multilayer by an electric current. *Phys. Rev. Lett.* **80**, 4281–4284 (1998).

3. Kiselev, S. I. *et al.* Microwave oscillations of a nanomagnet driven by a spin-polarized current. *Nature* **425**, 380–383 (2003).

4. Rippard, W., Pufall, M., Kaka, S., Russek, S. & Silva, T. Direct-current induced dynamics in $Co_{80}Fe_{10}/Ni_{80}Fe_{20}$ point contacts. *Phys. Rev. Lett.* **92**, 027201 (2004).

5. Krivorotov, I. N. *et al.* Time-domain measurements of nanomagnet dynamics driven by spin-transfer torques. *Science* **307**, 228–231 (2005).

6. Silva, T. J. & Rippard, W. H. Developments in nano-oscillators based upon spin-transfer point-contact devices. *J. Magn. Magn. Mater.* **320**, 1260–1271 (2008).

7. Kim, J.-V. Chapter four - spin-torque oscillators. In Robert E. Camley and Robert L. Stamps (ed.) *Solid State Physics*, vol. 63, chap. 4, 217–294 (Academic Press, 2012).

8. Bonetti, S., Muduli, P., Mancoff, F. & Åkerman, J. Spin torque oscillator frequency versus magnetic field angle: The prospect of operation beyond 65 GHz. *Appl. Phys. Lett.* **94**, 102507 (2009).

9. Berger, L. Emission of spin waves by a magnetic multilayer traversed by a current. *Phys. Rev. B* **54**, 9353–9358 (1996).

10. Slonczewski, J. C. Current-driven excitation of magnetic multilayers. *J. Magn. Magn. Mater.* **159**, L1–L7 (1996).

11. Ralph, D. C. & Stiles, M. D. Spin transfer torques. *J. Magn. Magn. Mater.* **320**, 1190–1216 (2008).

12. Kaka, S. *et al.* Mutual phase-locking of microwave spin torque nano-oscillators. *Nature* **437**, 389–392 (2005).

13. Mancoff, F. B., Rizzo, N. D., Engel, B. N. & Tehrani, S. Phase-locking in double-point-contact spin-transfer devices. *Nature* **437**, 393–395 (2005).

14. Silva, T. J. & Rippard, W. H. Developments in nano-oscillators based upon spin-transfer point-contact devices. *Journal of Magnetism and Magnetic Materials* **320**, 1260 – 1271 (2008).

15. Dumas, R. *et al.* Recent advances in nanocontact spin-torque oscillators. *IEEE Trans. Magn.* **50**, 4100107 (2014).

16. Ruotolo, A. *et al.* Phase-locking of magnetic vortices mediated by antivortices. *Nat. Nanotech.* **4**, 528–532 (2009).

17. Sani, S. *et al.* Mutually synchronized bottom-up multi-nanocontact spin torque oscillators. *Nat. Commun.* **4**, 2731 (2013).

18. Hoefer, M. A., Silva, T. J. & Stiles, M. D. Model for a collimated spin-wave beam generated by a single-layer spin torque nanocontact. *Phys. Rev. B* **77**, 144401 (2008).

19. Dumas, R. K. *et al.* Spin-wave-mode coexistence on the nanoscale: A consequence of the oersted-field-induced asymmetric energy landscape. *Phys. Rev. Lett.* **110**, 257202 (2013).

20. Demidov, V. E., Urazhdin, S. & Demokritov, S. O. Direct observation and mapping of spin waves emitted by spin-torque nano-oscillators. *Nature Mater.* **9**, 984–988 (2010).

21. Mohseni, S. M. *et al.* Spin torque generated magnetic droplet solitons. *Science* **339**, 1295–1298 (2013).

22. Slavin, A. & Tiberkevich, V. Spin wave mode excited by spin-polarized current in a magnetic nanocontact is a standing self-localized wave bullet. *Phys. Rev. Lett.* **95**, 237201 (2005).

23. Bonetti, S. *et al.* Experimental evidence of self-localized and propagating spin wave modes in obliquely magnetized current-driven nanocontacts. *Phys. Rev. Lett.* **105**, 217204 (2010).

24. Demidov, V. E. *et al.* Spin-current nano-oscillator based on nonlocal spin injection. *Scientific Reports* **5**, 8578– (2015).

25. Slonczewski, J. C. Excitation of spin waves by an electric current. *J. Magn. Magn. Mater.* **195**, L261–L268 (1999).

26. Madami, M. *et al.* Direct observation of a propagating spin wave induced by spin-transfer torque. *Nature Nanotech.* **6**, 635–638 (2011).

27. Slavin, A. & Tiberkevich, V. Theory of mutual phase locking of spin-torque nanosized oscillators. *Phys. Rev. B* **74**, 104401 (2006).

28. Pufall, M. R., Rippard, W. H., Russek, S. E., Kaka, S. & Katine, J. A. Electrical measurement of spin-wave interactions of proximate spin transfer nanooscillators. *Phys. Rev. Lett.* **97**, 087206 (2006).

29. Madami, M. *et al.* Propagating spin waves excited by spin-transfer torque: A combined electrical and optical study. *Phys. Rev. B* **92**, 024403 (2015).

30. Kendziorczyk, T., Demokritov, S. O. & Kuhn, T. Spin-wave-mediated mutual synchronization of spin-torque nano-oscillators: A micromagnetic study of multistable phase locking. *Phys. Rev. B* **90**, 054414 (2014).

31. Pogoryelov, Y. *et al.* Frequency modulation of spin torque oscillator pairs. *Appl. Phys. Lett.* **98**, 192501 (2011).

32. Lee, I. *et al.* Nanoscale scanning probe ferromagnetic resonance imaging using localized modes. *Nature* **466**, 845–848 (2010).

33. Urazhdin, S. *et al.* Nanomagnonic devices based on the spin-transfer torque. *Nature Nanotech.* **9**, 509–513 (2014).

34. Kruglyak, V. V., Demokritov, S. O. & Grundler, D. Magnonics. *J. Phys. D: Appl. Phys.* **43**, 264001 (2010).

35. Macià, F., Hoppensteadt, F. C. & Kent, A. D. Spin wave excitation patterns generated by spin torque oscillators. *Nanotechnology* **25**, 045303 (2014).

36. Izhikevich, E. M. & Hoppensteadt, F. C. Polychronous wavefront computations. *International Journal of Bifurcation and Chaos* **19**, 1733–1739 (2009).

37. Locatelli, N., Cros, V. & Grollier, J. Spin-torque building blocks. *Nature Mater.* **13**, 11–20 (2014).

38. Fell, J. & Axmacher, N. The role of phase synchronization in memory processes. *Nat. Rev. Neurosci.* **12**, 105 (2011).

39. Vansteenkiste, A. *et al.* The design and verification of MuMax3. *AIP Adv.* **4**, 107133 (2014).

Acknowledgements This work was supported by the European Commission FP7-ICT-2011-contract No. 317950 “MOSAIC”. It was also supported by the European Research Council (ERC) under the European

Communitys Seventh Framework Programme (FP/2007-2013)/ERC Grant 307144 “MUSTANG”. Support from the Swedish Research Council (VR), the Swedish Foundation for Strategic Research (SSF), and the Knut and Alice Wallenberg Foundation is gratefully acknowledged.

Authors contributions A.H. and P.D. fabricated the devices and A.H. performed all the electrical measurements. A.H. and E.I. performed the micromagnetic simulations. R.K.D. and J.Å. initiated and supervised the project. All authors contributed to the data analysis and co-wrote the manuscript.

Competing Interests The authors declare that they have no competing financial interests.

Correspondence Correspondence and requests for materials should be addressed to

R.K.D. (email: randydumas@gmail.com).